


Article

Four-Dimensional Trajectory Optimization for CO₂ Emission Benchmarking of Arrival Traffic Flow with Point Merge Topology

Chao Wang ^{*}, Chenyang Xu, Wenqing Li, Shanmei Li and Shilei Sun

College of Air Traffic Management, Civil Aviation University of China, No. 2898 Jinbei Road, Tianjin 300300, China; hhhjttqzhy@163.com (C.X.); cauclwq@163.com (W.L.); sm-li@cauc.edu.cn (S.L.); sl-sun@cauc.edu.cn (S.S.)

* Correspondence: wangch@cauc.edu.cn

Abstract: The benchmarking of CO₂ emissions serves as the foundation for the accurate assessment of the environmental impact of air traffic. To calculate the environmental benchmarks of arrival traffic flows with Point Merge System (PMS) patterns, this study proposes a 4D trajectory optimization method that combines data-driven and optimal control models. First, the predominant arrival routes of traffic flows are identified using the trajectory spectral clustering method, which provides the horizontal reference for 4D trajectory optimization. Second, an optimal control model for vertical profiles with point merging topology is established, with the objective of minimizing the fuel–time cost. Finally, considering the complex structure of the PMS, a flexible and adaptable genetic algorithm-based vertical profile nonlinear optimization model is created. The experimental results demonstrate that the proposed method is adaptable to variations in aircraft type and cost index parameters, enabling the generation of different 4D trajectories. The results also indicate an environmental efficiency gap of approximately 10% between the actual CO₂ emissions of the arrival traffic flow example and the obtained benchmark. With this benchmark trajectory generation methodology, the environmental performance of PMSs and associated arrival aircraft scheduling designs can be assessed on the basis of reliable data.

Keywords: air traffic management; 4D trajectory optimization; continuous descent operation; genetic algorithm; trajectory clustering; point merge system



Citation: Wang, C.; Xu, C.; Li, W.; Li, S.; Sun, S. Four-Dimensional Trajectory Optimization for CO₂ Emission Benchmarking of Arrival Traffic Flow with Point Merge Topology. *Aerospace* **2024**, *11*, 673. <https://doi.org/10.3390/aerospace11080673>

Academic Editor: Roberta Fusaro

Received: 13 June 2024

Revised: 10 August 2024

Accepted: 12 August 2024

Published: 16 August 2024



Copyright: © 2024 by the authors. Licensee MDPI, Basel, Switzerland. This article is an open access article distributed under the terms and conditions of the Creative Commons Attribution (CC BY) license (<https://creativecommons.org/licenses/by/4.0/>).

1. Introduction

With the demand for air travel increasing after the COVID-19 pandemic, the environmental impacts caused by air traffic have become increasingly serious. Previous research [1] has suggested that aviation accounts for 2.5% of global CO₂ emissions. Nevertheless, it has been demonstrated to contribute approximately 4% to the global warming observed to date. For the sustainable development of the aviation and commercial aircraft manufacturing industries, many new technologies that can reduce carbon emissions have been extensively explored. Among the numerous measures aimed at reducing CO₂ emissions from aviation, enhancing the environmental performance of air traffic systems is currently regarded as the most viable, significant, and promising approach.

In the National Airspace System, a Terminal Maneuvering Area (TMA) is a complex area of airspace surrounding one or more metropolitan airports, designed to aggregate arriving traffic flows from different directions. To increase the capacity of TMAs, an arrival route structure based on area navigation, called the Point Merge System (PMS), has been developed to assist controllers in sequencing and reducing open-loop radar vectoring. A PMS is a method for delaying aircraft involving less radar vectoring. Its structure includes a merge point and equidistant arc-shaped sequencing legs to the merge point. The flight path in a PMS can be lengthened or shortened as needed without radar vectoring. In the future Global Air Navigation Plan of ICAO [2], the PMS is recognized as having the potential to

reduce environmental impacts. However, a well-defined, scientific emissions benchmark for the minimum harmful input under a given air traffic flow is still lacking. Therefore, a scientifically accurate benchmark for measuring environmental performance is needed. With such a benchmark, low-carbon aircraft scheduling techniques can be applied in a step-by-step manner.

In order to better understand the environmental impacts of TMAs, both at present and in the future, one approach being adopted by Air Traffic Management (ATM) operators is quantifying their performance using measures of flight inefficiency [3]. Flight inefficiency can be defined as anything that causes an aircraft to fly a path different from its fuel-optimal four-dimensional trajectory. Therefore, the accuracy of the optimized flight trajectory is important. A challenge posed in the evaluation of the environmental impact of air traffic, both at present and in the future, is determining the optimal trajectory and minimal fuel burn (which is the benchmark for fuel-based inefficiency analysis) for any given route, especially for arrival routes within a TMA.

This research encompasses two technical aspects. First, the arrival traffic flow with a point merge pattern is identified from the cluttered trajectories within the terminal area, and prevalent arrival routes are further extracted. Second, as continuous descent operations are recommended by the ICAO, descent profile optimization provides an important basis for CO₂ emission benchmarking studies. A literature survey on these two technical aspects is provided below.

The implementation of new airspace surveillance technologies, such as Automatic Dependent Surveillance-Broadcast (ADS-B), has led to improvements in the integrity, quality, and accessibility of aircraft tracks. The analysis of track records is becoming a viable method for identifying traffic patterns and assessing the operational performance of air traffic. At present, trajectory clustering is becoming the most effective method for achieving these goals. Various distance-based clustering algorithms have been reported, but the core component of all of them is the similarity or distance measure used for the classification of data [4].

In order to accurately represent the overall similarity between two trajectories, various spatial distance-based similarity metric models have been proposed. Almost all of the typical clustering algorithms can be used, either directly or synthetically, to perform trajectory clustering using pre-computed similarity values [5]. Besse et al. summarized the calculation of spatial distances of trajectories for clustering, giving the distances between sets of points, between points and line segments, and between line segments. This new distance was compared to other metrics, according to the corresponding clustering results obtained using both hierarchical clustering and affinity propagation (AP) methods [6]. Poppe and Buxbaum clustered aircraft climb trajectories using the k-means algorithm, where the resulting clusters could further be used in trajectory prediction applications [7]. The calculated point-to-segment distance matrix—a spectral clustering algorithm—has been adopted to cluster flight trajectories [8].

Given the limitations of distance measures for high-dimensional spatio-temporal trajectories, researchers have attempted to improve the credibility of trajectory similarity through dimensional reduction. For example, Olive and Morio used the Douglas–Pecuker algorithm to approximate the original trajectories according to a fixed step size [9]. Xuhao et al. revealed the time-series nature of the trajectories, converted the trajectories into a time-series of headings relative to their remaining distances, and calculated the similarity between them using the dynamic time warping algorithm [10]. In recent years, the continuous development of Deep Learning approaches has demonstrated their powerful ability to extract internal potential features from large data sets. Deep autoencoders have been developed to train deep neural networks in order to learn suitable representations from high-dimensional trajectory data. Subsequently, the output of the Deep autoencoder is input into a GMM or DNSCAN for clustering [11]. In order to understand the spatial distribution characteristics of the arrival traffic flow in a TMA, Wang established a flight

trajectory feature compression model on the basis of the t-SNE method, following which the density peaks clustering approach was used to extract the prevailing traffic flow [12].

Trajectory clustering plays a crucial role in air traffic management, providing insights for airspace structure optimization, trajectory planning, and trajectory prediction. The application of trajectory clustering in the field of traffic pattern recognition within TMAs is evolving and expanding, including enhancement of the airspace structure around airports [13], examination of the reliability of arrival and departure route networks [14], and analysis of the efficiency of air traffic operations [9]. However, due to the structural complexity of the point merging procedure and the eventual convergence of arrival traffic, which causes flight trajectories to be more mixed, aggregated, and intertwined, identification of traffic flows with PMS topology and its representative trajectories may require a new similarity-measuring model that takes into account the complex features of arrival traffic trajectories.

Trajectory optimization plays a key role in ensuring the success of trajectory-based operations. The optimization problem for 4D aircraft trajectories has been studied extensively by many scholars, who have gradually realized that the 4D trajectory optimization problem can be formulated as a multi-phase optimal control problem with process constraints, terminal points constraints, and control constraints [15,16]. At present, 4D trajectory optimization methods can be classified into four categories: dynamic programming, indirect, direct, and meta-heuristic algorithms.

Initially, researchers explored the potential of dynamic programming methods to address trajectory optimization problems [17]. However, it was found that the computational complexity and issues associated with interpolation limited the applicability of these methods in practical trajectory optimization scenarios [18]. Many scholars have attempted to address the aforementioned limitations of dynamic programming methods [19–21]. For example, Ahmed et al. [22] recently proposed a modified dynamic programming method which overcomes the curse of dimensionality and the extended mesh problem while enhancing the computational efficiency and feasibility of 4D trajectory optimization.

Indirect methods are based on transforming the 4D trajectory optimal control problem into a Hamiltonian boundary value problem, which is then solved using numerical methods to obtain differential or algebraic equations [23,24]. The primary application of this technique is to optimize relatively simple systems [25]. Indirect methods encounter difficulties in solving the trajectory optimization problem due to the complex model dynamics and the numerous constraints involved in the 4D trajectory optimization problem [26].

Compared with indirect methods, direct methods discretize the complex optimal control model into a finite-dimensional nonlinear planning problem, which has higher computational efficiency and numerical stability, and is suitable for optimal control problems with complex constraints [27,28]. Soler et al. [29] have transformed the 4D trajectory optimization problem into a multi-stage optimal control problem and used the point collocation method to obtain a 4D trajectory with the objective of minimum fuel consumption. Based on this study, Soler et al. [30] further analyzed the performance of aircraft, considering different take-off weights and cost indices to obtain a 4D trajectory with minimum fuel consumption. Bonami et al. [31] transformed the 4D trajectory optimization problem into a mixed-integer nonlinear programming problem and used the branch and bound method to find a 4D trajectory with the objective of optimal fuel consumption.

Continuous Descent Operations (CDOs) have been recognized as an effective way to significantly reduce fuel burn and CO₂ emissions in aircraft operations [32]. By keeping arriving aircraft at their cruise altitude longer, then following a continuous descent at near-idle thrust with no level-flight segments, CDO can bring substantial fuel savings and environmental benefits [33]; therefore, it has become a globally recommended emission mitigation practice by the International Civil Aviation Organization (ICAO).

The pseudo-spectral method is a representative direct method that transforms the continuous optimal control problem into a nonlinear programming (NLP) problem, enabling more efficient parameterization of constraints. Many scholars have employed pseudo-

spectral methodologies to address the descent profile optimization problem, in accordance with specified horizontal route conditions. For instance, Park and Clarke divided a CDO into a number of descent stages according to different flap settings and calibrated airspeed constraints, then modeled the trajectory optimization problem as a multi-phase optimal control problem between two previously known endpoints, and solved for the optimal continuous descent trajectory using the Gaussian pseudo-spectral method [34]. Subsequently, Park et al. employed the Legendre–Gauss pseudo-spectral method to determine the optimal commencement of the descent point and descent profile, and proposed a CDO trajectory that simultaneously reduces flight time and minimizes fuel consumption [35]. Similarly, Ma et al., taking delay time, fuel burn, and aircraft noise as objectives, used the Legendre–Gauss pseudo-spectral method to generate optimized trajectories [36]. Zhu et al. developed trajectory optimization models based on the Gaussian pseudo-spectral method to obtain optimal descent trajectories for different cost index values [37]. Most of the above studies relied on the GPOPS toolbox for solutions. However, the quality of the solution and the convergence of the computational process depends heavily on the initial estimates of the control variables, and inappropriate values can lead to solution failure [38].

The advent of swarm intelligence optimization technology has prompted some scholars to employ heuristic algorithms in an attempt to resolve the optimal control problem of 4D trajectories. Yang et al. addressed the challenge of not being able to provide time-continuous control variables in trajectory optimization problems by transforming the optimal control problem into a nonlinear planning problem [39]. The nonlinear planning model was constructed using the thrust and load factor as decision variables, which was solved using IPSO-SQP [40]. They claimed that, despite its simplicity and intuitiveness, the particle swarm methodology proved to be quite effective in finding the optimal solution to orbital rendezvous optimization problems with considerable numerical accuracy. Ren et al. developed an integer planning model based on flight segment division and employed a particle swarm optimization algorithm to obtain optimal green trajectories [41].

Although the aforementioned studies have achieved notable success in their respective fields, they have not yet addressed the CO₂ emissions baseline trajectory problem of traffic flow. In order to investigate the mechanism driving the environmental inefficiency of point merge traffic flows within a busy terminal area, we combine trajectory clustering and optimal control methods to propose a 4D trajectory optimization model for benchmarking the CO₂ emissions of inbound traffic flows. This is the first time that such a systematic approach has been utilized to gain insight into the emissions benchmarking of traffic flows from the perspective of a data-driven optimization model.

The differences between the research in this study and the existing achievements are specifically reflected in three aspects: First, the continuous descent operation under the special structure of the PMS presents distinct constraints from traditional arrival procedures. To satisfy these constraints, we propose a new optimal control model for the 4D arrival trajectory optimization problem. Second, a 4D trajectory nonlinear optimization method is developed on the basis of a genetic algorithm to solve the 4D trajectory optimal control problem. The method is able to model and solve the PMS vertical profile encompassing a level-flight arc leg in an ad hoc manner. Third, a spherical segment–path distance between trajectories directly using their coordinates is calculated, which overcomes the deformation defects caused by the indirect use of map projection coordinates.

To establish environmental benchmarks for arrival traffic flows utilizing PMS topology, this study introduces a 4D trajectory optimization method that integrates data-driven and optimal control models. The predominant arrival routes are identified via trajectory spectral clustering. A tailored optimal control model, specifically designed for the vertical profiles of PMS topology, is developed with the objective of minimizing fuel–time costs, using the identified arrival routes as horizontal guidance. To overcome the limitations of traditional solvers like GPOPS in addressing optimal control problems involving multiple descent processes, a genetic algorithm-based solution approach is proposed. Subsequently, the proposed method was applied to a realistic terminal airspace scenario, and its applicability

was validated through two consecutive experiments: one for identifying arrival traffic flows and the other for optimizing 4D trajectories.

2. Methodology

The section outlines the process of data pre-processing, point merge operation flow identification, and continuous descent operation 4D trajectory generation, as illustrated in Figure 1. The process consists of five steps: (1) extract arrival trajectories from the traffic flow records within the boundaries of the terminal control area; (2) calculate the distances between pairs of trajectories sequentially to obtain the spherical symmetric segment distances, and construct the similarity matrix of the arrival trajectory set; (3) use a spectral clustering algorithm to obtain the spatial pattern of arrival traffic flow, identify the core trajectories for the identified traffic flow and, finally, take the horizontal profile of the core trajectory as the prevailing arrival route; (4) establish an optimal control model for a CDO profile with PMS topology based on predominant arrival routes; and (5) solve the optimal control problem for vertical profiles using a nonlinear trajectory optimization model—called GACDO—based on a genetic algorithm.

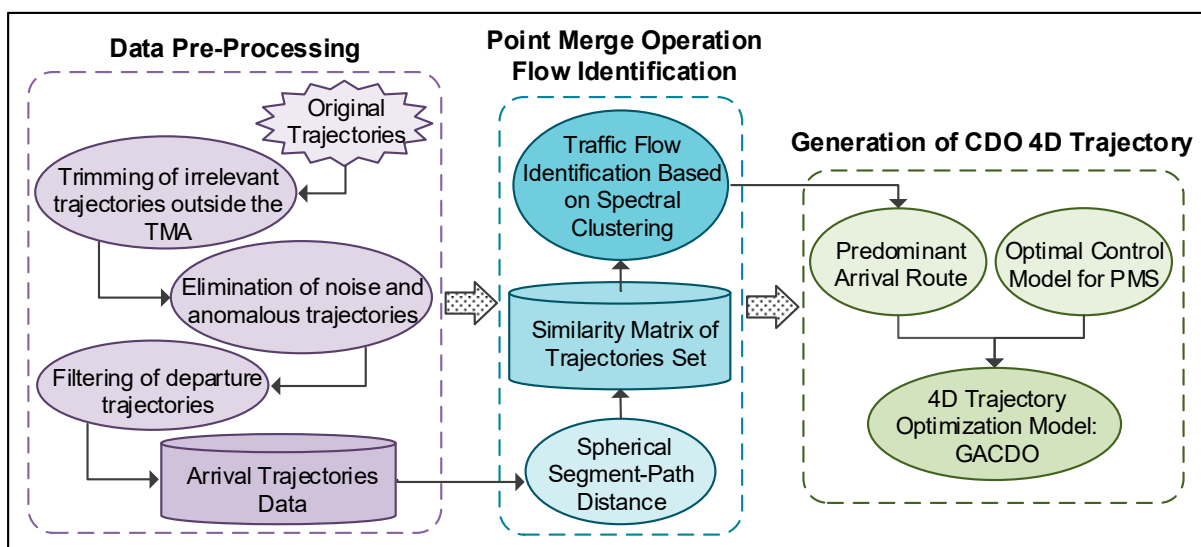


Figure 1. The framework of the proposed method.

2.1. Data Pre-Processing

Air traffic surveillance equipment, such as secondary surveillance radar and ADS-B, are capable of acquiring many kinds of aircraft navigational traffic data, such as the position, altitude, speed, and heading of aircraft in the terminal area and their changes, in real-time. The Air Traffic Control (ATC) automation system receives, processes, and displays the surveillance data and, at the same time, records all or part of the flight tracks of the aircraft.

The concepts of track and trajectory are not distinguished in ATC operations and research and, for the purpose of this study, they are defined as follows:

A basic track is the geographic position and altitude information of the k th point of an aircraft i recorded by a surveillance sensor at a certain time t , expressed as a four-dimensional vector $P_k = (\alpha_k, \beta_k, h_k, t_k)$, where α_k , β_k , and h_k denote the longitude, latitude, and altitude of the aircraft in space, respectively, and t denotes the timestamp.

The trajectory is the historical trace of an aircraft's flight over a period of time, which is actually a continuous curve. Due to the data processing cycle of monitoring sensors and the cognitive limitations of air traffic controllers, the trajectory T consists of a series of discrete tracks arranged in chronological order with certain time intervals; that is, $T = (P_1, P_2, \dots, P_k, \dots, P_K)$, where $k \in [1, K]$ is the chronological index of tracks and K is the total number of tracks in the trajectory T .

Suppose that the set of trajectories formed by all arriving aircraft in the terminal area in a given time period is $\Gamma = \{T_1, T_2, \dots, T_i, \dots, T_N\}$, where each T_i denotes an arriving flight trajectory and N denotes the total number of all trajectories.

Although the trajectory data recorded by ATC surveillance systems has been processed for correlation, noise reduction, and elimination of duplicates, it still contains a large number of redundant and irrelevant tracks in the context of analyzing the environmental performance of the arriving traffic flows.

Most trajectories also contain tracks of the en-route flight, or even of the entire flight phase from takeoff to landing. It is necessary to remove those tracks outside of the terminal airspace. The geographic boundary of the terminal airspace is usually formatted as a two-dimensional polygon. For such processing, tracks outside the boundary of this polygon can be eliminated, while those inside are retained.

Tracks within the terminal airspace may also contain overflying aircraft tracks. In addition, there are general aviation flights and training flights within the terminal airspace. When general aviation aircraft are equipped with ADS-B transmitters, the surveillance system will also record these tracks. We can eliminate these tracks through determining whether the aircraft lands at the major airport in the terminal airspace. As there are different movement patterns for arriving and departing flights, they need to be distinguished. Arrival and departure trajectories can be easily separated according to their departure and destination airports in the flight plans that correspond to the trajectories.

Finally, we obtain the arrival trajectories during a period of time. The set of trajectories formed by all arriving aircraft in the terminal area over a given time period is $\Gamma = \{T_1, T_2, \dots, T_i, \dots, T_N\}$, where each T_i denotes an arriving flight trajectory and N denotes the total number of all such trajectories.

2.2. Traffic Flow Identification and Predominate Arrival Route Recognition

Arrival traffic flow consists of successive arrivals with similar movement behaviors. As they have similar trajectories, they are often recognized through trajectory clustering. In general, clustering can be performed through comparing trajectory objects. Therefore, it is important that a trajectory distance measurement model reflects the trajectory shape characteristics, including the physical distance and total length of the trajectory. In addition, as aircraft fly over a large area of the Earth's surface, the trajectory distance must take into account its spherical geometry in order to avoid the deformation caused by map projection.

2.2.1. Spherical Segment–Path Distance between Trajectories

Supposing that there are two tracks, $P_1(\lambda_1, \phi_1, h_1, t_1)$ and $P_2(\lambda_2, \phi_2, h_2, t_2)$, where λ_1 and ϕ_1 represent the longitude and latitude of P_1 , and λ_2 and ϕ_2 represent the longitude and latitude of P_2 , the shortest distance between them can be calculated using the Haversine formula [42], as shown in Equation (1):

$$\widehat{d}_{gc}(P_1, P_2) = 2R_0 \arcsin \sqrt{\sin^2\left(\frac{\phi_2 - \phi_1}{2}\right) + \cos(\phi_2) \cos(\phi_1) \sin^2\left(\frac{\lambda_2 - \lambda_1}{2}\right)} \quad (1)$$

where R_0 represents the average radius of the Earth. This formula takes into account the rounding error in the proximity between the two points and calculates the great circle distance between them.

If trajectory T_2 has a segment arc $\widehat{S}k$ defined by its endpoints P_k and P_{k+1} , the great circle distance from any track point O on trajectory T_1 to arc $\widehat{S}k$ can be calculated with Equation (2):

$$\widehat{d}_{ps}(O, \widehat{S}) = \min(\widehat{d}_{gc}(O, P_k), \widehat{d}_{gc}(O, P_{k+1})) \quad (2)$$

Figure 2a shows the distance $\widehat{d}_{pT}(O, T_2)$ from point O to trajectory T_2 , which is the minimum distance between the point O and all segments that make up T_2 . This can be calculated using Equation (3):

$$\widehat{d}_{pT}(O, T_2) = \min \widehat{d}_{pS}(O, S_k) \quad k \in [1, 2, \dots, K_2 - 1], \quad (3)$$

where K_2 is the number of tracks contained in T_2 . Then, the spherical segment–path distance from T_1 to T_2 can be defined as Equation (4):

$$\widehat{d}_{SPD}(T_1, T_2) = \frac{1}{K_1} \sum_{k=1}^{K_1} \widehat{d}_{pT}(O_k, T_2) \quad (4)$$

where O_k is the k th track on trajectory T_1 and the number of track points contained in trajectory T_1 is K_1 . A schematic representation of the calculation of $\widehat{d}_{SPD}(T_1, T_2)$ is provided in Figure 2b.

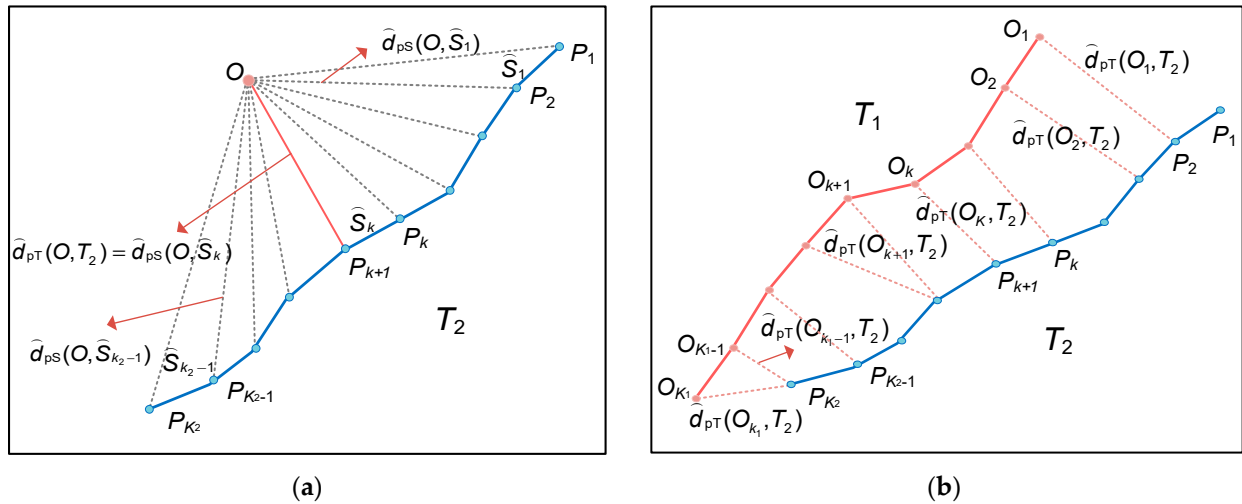


Figure 2. Spherical segment–path distance between trajectories: (a) the distance from point O to trajectory T_2 ; (b) the spherical segment–path distance from T_1 to T_2 .

The inter-trajectory distance matrix $D = [d_{ij}]_{N \times N}$ is generated by calculating the symmetric unidirectional great circle distance between trajectories T_i and T_j in the set of arrival trajectories Γ , as shown in Equation (5).

$$d_{ij} = \frac{1}{2} (\widehat{d}_{SPD}(T_i, T_j) + \widehat{d}_{SPD}(T_j, T_i)) \quad (5)$$

2.2.2. Predominant Arrival Route Recognition

Spectral clustering is an algorithm derived from graph theory, the main idea of which is to treat all data as points in a high-dimensional space connected by edges. The weight of an edge between two distant points is low, while the weight of an edge between two close points is high. Clustering can then be achieved through dividing the graph of data points into sub-graphs in such a way that the sum of edge weights between the sub-graphs is minimized and the sum of edge weights within the sub-graphs is maximized.

The matrix of trajectory similarity is constructed based on inter-trajectory distances, in order to accurately reflect the similarity relationship between data points. This results in higher similarity between similar points and lower similarity between dissimilar points.

Equation (6) shows the Gaussian kernel function $\omega_{i,j}$ used to construct the similarity between trajectories T_i and T_j :

$$\omega_{i,j} = \exp\left(-\frac{(d_{i,j})^2}{2\sigma}\right), \quad i = 1..N, j = 1..N. \quad (6)$$

The parameter σ in Equation (6) controls the width of the neighborhood; a larger value of σ indicates a higher similarity between the trajectories, which should be adjusted according to the specific situation. A non-negative link weight unidirectional graph G can be constructed on the basis of the similarity between the trajectories. The weight of the zero eigenvalue of the Laplace matrix L of the graph G is approximately equal to the number of connected sub-graphs of the graph G , denoted as Z . It is important to note that Z represents the estimated number of clusters.

The spectral clustering method divides the original trajectory samples into Z subsets (i.e., Z different clusters of trajectories) according to their similarities in structure and proximity to each other. However, in practice, the clusters obtained from preliminary clustering do not accurately reflect the spatial characteristics of the traffic flow. This is because the distances between trajectories within the clusters are not the same, especially when the clusters contain some abnormal trajectories. Thus, it is often necessary for a cluster to be subdivided into several smaller sub-clusters. This study proposes the use of a k -Nearest Neighbor (KNN) distance model between the trajectories to identify prevalent, anomalous, and representative trajectories obtained from the same cluster. The aim is to identify the main trajectories and their representative flight routes, which can effectively express the characteristics of the spatial distribution of traffic flow.

To obtain the average KNN distance of a trajectory T_i in the trajectory cluster F_z , the inter-trajectory distance matrix D —given by Equation (5)—is first searched to find the distances to other trajectories in F_z . Then, these distances are sorted from smallest to largest, and the average KNN distance \bar{d}_i of T_i is calculated using Equation (7):

$$\bar{d}_i = \frac{\sum_{j=1}^K d_{i,j}}{K}. \quad (7)$$

The k -nearest neighbor distance matrix of T_i also can be used to classify a given cluster of trajectories into two sub-classes using k -medoids. This process yields the prevalent traffic flow trajectories and the anomalous trajectories. Each class of data obtained using the k -medoids classification algorithm has a corresponding center that serves as a representative of the data with high similarity. The prevalent traffic flow trajectories also exhibit a core trajectory, which represents the most frequent movement patterns under specific operating conditions, such as air traffic flow, traffic mix, runway-in-use configuration, and meteorological conditions. It serves as a horizontal reference for arrival routes during the following 4D trajectory optimization.

2.3. Optimization of Continuous Descent 4D Trajectory with Point Merge Pattern

2.3.1. Continuous Descent Operation in Point Merge System

The PMS is a new type of arrival route structure based on satellite navigation, proposed by the European Organization for the Safety of Navigation (EUROCONTROL). It provides a systematic method for the sequencing and continuous descent of arriving aircraft, and has been gradually adopted worldwide in recent years. A typical point merging system consists of inner and outer sequencing arc legs and a merge point (MP), as shown in Figure 3. An arc leg is a segment of arc with equal distance from the merge point, which is used to regulate the spacing of successive aircraft. For the purpose of establishing sufficient vertical separation, the inner arc is generally higher than the outer arc by several flight levels, and aircraft are required to maintain the same altitude and constant speed while on the arc. The merge point is an orientation point designed within the terminal area. Aircraft arriving

from different directions fly into the arc leg from their arrival routes and turn directly to the merge point upon receiving turning instructions from air traffic controllers.

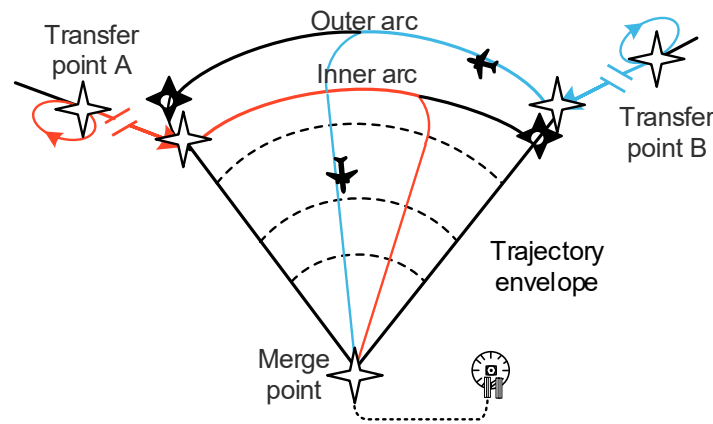


Figure 3. Route structure of point merge system.

When an aircraft passes through the merge point, it will fly along a short segment to the final approach fix. The most important task for the pilot of the aircraft during this period is to smoothly and quickly intercept the Instrument Landing System (ILS) localizer. There is no need to optimize the trajectory at this segment and, so, the MP is used as the end of the CDO. Figure 4 shows a typical CDO descent profile, combining the route structure of the point merge procedure and the basic requirements of the CDO. The diagram shows the relationship between flight distance to the MP, flight time to the MP, and flight altitude.

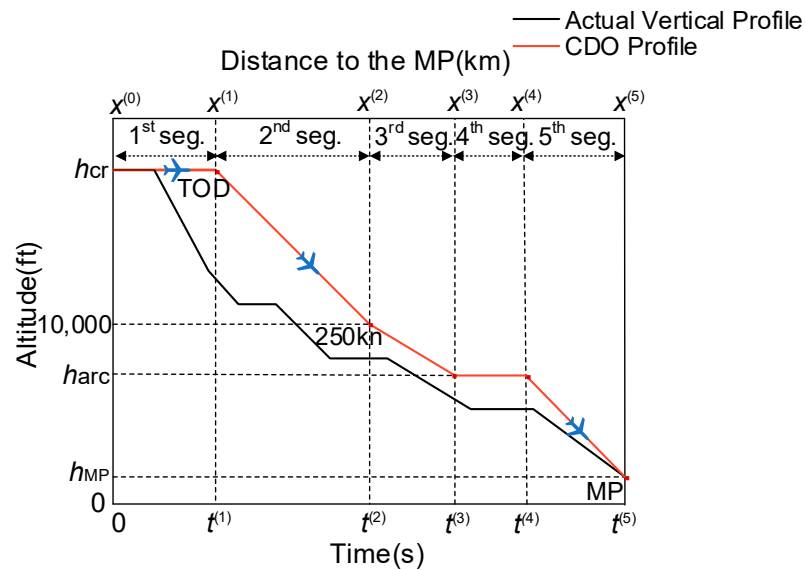


Figure 4. Typical CDO process of point merge procedure.

The descent can be broken down into five phases, according to standard airline operation procedures and the special structure of the point merge procedure. During phase 1, the aircraft maintains a constant Calibrated Airspeed (CAS) at the flight level while entering the terminal airspace, until it reaches the Top of Descent (TOD). The regulations for operating large commercial aircraft require that the CAS of an aircraft must not exceed 250 knots below 10,000 ft. Additionally, air traffic control mandates that the CAS of an aircraft must not be less than 250 knots above 10,000 ft. Therefore, during phase 2, the aircraft must descend to 10,000 ft and decelerate to 250 knots. In phase 3, the aircraft descends to the specified altitude of the sequencing arc and decelerates to the specified

speed limit of the arc. During phase 4, the aircraft flies along the arc while maintaining a constant speed and altitude. In phase 5, the aircraft leaves the sequencing arc and gradually descends to the specified altitude and decelerates to restricted speed at the MP.

In this section, we employed spectral clustering to identify the traffic flow with the PMS pattern and to obtain the core route of this traffic flow. This core route represents the horizontal trajectory of the aircraft among this traffic flow, thereby providing a horizontal reference for 4D trajectory optimization of the arriving aircraft. Subsequently, we optimize the vertical profile of this core route based on the five phases illustrated in Figure 4. As such, the horizontal route and its optimal vertical profile constitute the complete 4D trajectory.

2.3.2. Optimal Control Model for Point Merge Pattern

The optimization problem for the CDO vertical profile in point merge operations can be transformed into a multi-stage nonlinear optimal control problem, given the initial conditions of horizontal route, aircraft type, arrival altitude, and speed. The relevant constraints are determined according to air traffic rules depending on the given horizontal distance of the arrival route and the length of the sequencing arc. A multi-stage nonlinear optimal control model of the CDO profile is then established in order to meet the requirements of the point merge systems.

(1) Objective function

There is a simple proportional relationship between aircraft fuel consumption and CO₂ emissions [43]. The CO₂ emission index of aviation kerosene is 3.15; that is, 3.15 kg of CO₂ is produced for every 1 kg of fuel burned. Therefore, the objective of minimum CO₂ emissions can be mapped to fuel consumption optimization. The objective function is given as Equation (8):

$$\min J_{\text{fuel}} = f^{(1)} \times \frac{(x^{(1)} - x^{(0)})}{v_T^{(1)}} + f^{(4)} \times \frac{(x^{(4)} - x^{(3)})}{v_T^{(4)}} + \sum_{p=2,3,5} \int_{t_f^{(p)}}^{t_0^{(p)}} f^{(p)} dt \quad (8)$$

Meanwhile, air traffic control aims to expedite air traffic flow while minimizing flight time. The objective function is shown in Equation (9):

$$\min J_{\text{time}} = t_f^{(5)} \quad (9)$$

In these equations, the fuel consumption rate for phase p is represented by $f^{(p)}$, while $v_T^{(p)}$ denotes the level flight true airspeed of the aircraft during the same phase. Additionally, $x^{(p)}$ represents the distance to be flown from the end of phase p to the MP, and $t_f^{(5)}$ indicates the end moment of the CDO.

Typically, in the actual operation of a commercial aircraft, fuel and time-related costs are considered together through setting a Cost Index (CI) in the Flight Management System (FMS). Thus, an economic cruising speed that minimizes the total Direct Operating Cost (DOC) is obtained. The objective function is shown in Equation (10):

$$\min J_{\text{DOC}} = J_{\text{fuel}} + CI \times J_{\text{time}} \quad (10)$$

(2) Control Variables

In the optimal control model, the aircraft state \mathbf{X} is defined in terms of the distance to the MP x , the altitude h , and the true airspeed v_T . Therefore, $\mathbf{X} = [x, h, v_T]$. The force analysis of the aircraft descent is used to calculate each variable of the flight state, as shown in Equation (11):

$$\begin{cases} \frac{dv_T}{dt} = \frac{T-D}{m} - g \sin \gamma \\ \frac{dh}{dt} = v_T \sin \gamma \\ \frac{dx}{dt} = v_T \cos \gamma \end{cases} \quad (11)$$

Equation (12) is used to calculate T (engine thrust) and D (drag), where m is the mass of the aircraft and g denotes the gravitational acceleration:

$$\begin{cases} T = C_{\text{des}} \times C_{T1} \times \left(1 - \frac{h}{C_{T2}} + C_{T3} \times h^2\right) \\ D = \frac{[C_{D0} + C_{D2} \times \left(\frac{2mg}{\rho v_T^2 S_w}\right)] \times \rho v_T^2 S_w}{2} \end{cases} \quad (12)$$

where C_{des} represents the thrust correction coefficient, C_{T1} represents the first thrust coefficient, C_{T2} represents the second thrust coefficient, C_{T3} represents the third thrust coefficient, C_{D0} represents the zero-lift drag coefficient, C_{D2} represents the induced drag coefficient, ρ represents the atmospheric density, and S_w represents the reference area of the wing. These coefficients are related to the aircraft type, and can all be derived from the aircraft parameters in the BADA documents [44].

According to Equation (12), the thrust of an aircraft during descent is solely dependent on its altitude in an ideal scenario. As the descent angle γ determines the aircraft state, it may be considered as a unique control variable.

(3) Constraints

The values of state variables (e.g., flight distance and altitude) in each phase must be restricted to a corresponding range, as shown in Equation (13).

$$\begin{cases} x^{(5)} = 0 \\ h_0^{(1)} = h_{\text{cr}} \\ h_f^{(2)} = 10,000 \text{ ft} \\ h_0^{(4)} = h_{\text{arc}} \\ h_f^{(5)} = h_{\text{MP}} \end{cases} \quad (13)$$

where $h_0^{(p)}$ represents the initial altitude for phase p , $h_f^{(p)}$ represents the final altitude for phase p , h_{cr} represents the handover altitude when the aircraft enters the terminal airspace, and h_{MP} represents the altitude when the aircraft is at its MP.

Equation (14) shows the corresponding speed restrictions that the aircraft must satisfy in different phases when descending within the terminal airspace:

$$\begin{cases} 250 \leq v_C^{(p)} \leq v_{\text{MO}}, p \in [1, 2] \\ v_{\text{C,MP}} \leq v_C^{(p)} \leq 250 \text{ kn}, p \in [3, 4] \\ v_C^{(4)} = v_{\text{C,arc}} \\ v_f^{(5)} = v_{\text{C,MP}} \end{cases} \quad (14)$$

where $v_C^{(p)}$ represents the calibrated airspeed of the aircraft in phase p , v_{MO} is the maximum allowable CAS of the aircraft, $v_f^{(p)}$ is the CAS at the end of phase p , and $v_{\text{C,MP}}$ is the CAS at the MP.

To avoid an uncomfortable situation for passengers caused by a high descent rate, the glide path angle γ must be limited to a certain range, as shown in Equation (15):

$$\gamma_{\text{min}} \leq \gamma \leq \gamma_{\text{max}} \quad (15)$$

where γ_{min} and γ_{max} are the upper and lower limits of the glide path angle, respectively.

Although the optimal control model divides the complete flight into several independent phases, it is important to maintain consistency between the states before and after the critical point of the artificially divided successive segments, as shown in Equation (16):

$$X_f^{(p-1)} = X_0^{(p)} \tag{16}$$

where $X_0^{(p)}$ and $X_f^{(p)}$ denote the initial and final states of the aircraft in phase p , respectively.

2.3.3. GACDO Algorithm for Point Merge Pattern

The challenge in solving the optimal control model for continuous descent operations lies in the uncertainty regarding the future flight time. To address this issue, we use the exemplar trajectory identified in Section 2.2 as the reference route, and choose the horizontal flight distance as one of the key decision variables for modelling.

Most airlines have developed operating procedures for various aircraft types, in order to enhance their economic efficiency, safety, and passenger comfort. These procedures offer clear guidance on the CAS profile of the aircraft, as illustrated in Figure 5. This study models the CAS profile of the arrival process using seven decision variables, denoted by $S = [s_1, s_2, s_3, s_4, s_5, v_1, v_2]$. Figure 5 shows that v_1 represents the extreme CAS for the second phase, while v_2 represents the CAS when the aircraft is flying on the sequencing arc. The notation used in this context is as follows: s_1 represents the distance of the level flight segment before the top of descent (TOD); s_2 represents the distance flown by the aircraft as it changes from its initial speed to v_1 ; s_3 represents the distance flown by the aircraft as it maintains v_1 ; s_4 represents the distance flown by the aircraft as it decreases from v_1 to 250 kn; and s_5 represents the distance flown by the aircraft as it descends from an altitude of 10,000 ft to the sequencing arc altitude.

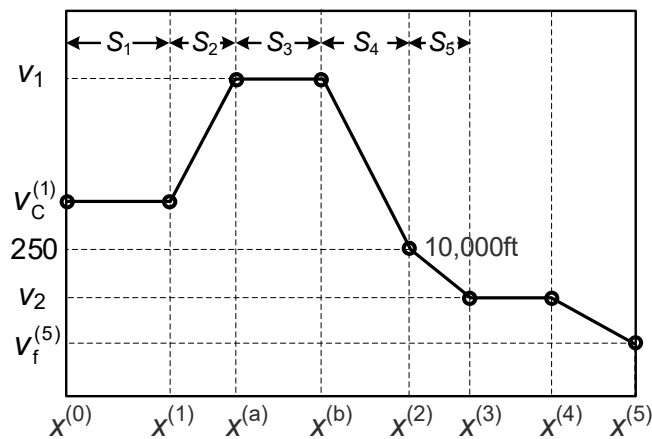


Figure 5. Arrival CAS profile model, represented by seven decision variables.

Thus, the optimization model for the vertical profile is established as shown in Equation (17):

$$\begin{aligned} & \min f^*(s_1, s_2, s_3, s_4, s_5, v_1, v_2) \\ & \text{s.t.} \\ & \left\{ \begin{aligned} & s_1 + s_2 + s_3 + s_4 \leq x^{(3)} - x^{(0)} - 2 \\ & 1 \leq s_j \leq 80, j = 1, 2, 3, 4 \\ & v_{1,\min} \leq v_1 \leq v_{1,\max} \\ & v_{2,\min} \leq v_2 \leq v_{2,\max} \\ & s_j \in Z \quad j = 1, 2, 3, 4 \\ & v_j \in Z \quad j = 1, 2 \end{aligned} \right. \tag{17} \end{aligned}$$

The objective function is represented by $f^*(S)$, while $x^{(3)}$ represents the flight distance from the beginning of the sequencing arc to the MP. The minimum value of s_5 is constrained to 2 NM by $x^{(3)} - x^{(0)} - 2$. To facilitate aircraft operations, decision variables are typically constrained to integer values.

During level flight, the aircraft maintains a constant CAS, resulting in linearly varying fuel consumption with flight distance. However, during the descent phase, the fuel consumption is nonlinearly related to the flight distance due to the complex model dynamics. To solve this nonlinear objective function during aircraft descent, a numerical solution method is proposed.

The descent between the interval $[x^{(1)}, x^{(3)}]$ is used as an example to illustrate the numerical solution algorithm for fuel consumption. There are five known data points—namely, $(x^{(1)}, v_C^{(1)})$, $(x^{(a)}, v_1)$, $(x^{(b)}, v_1)$, $(x^{(2)}, 250)$, $(x^{(3)}, v_2)$, and $(x^{(4)}, v_2)$ —from the aircraft velocity profile shown in Figure 5. Similarly, dividing the interval $[x^{(1)}, x^{(3)}]$ by a sufficiently small distance Δx will produce a number of query points x_i , $i = [1, 2, \dots, N_1]$, where N_1 denotes the number of query points. Assuming that the CAS is uniformly decreasing, a linear interpolation method can be used to generate the calibrated airspeed corresponding to any query point x_i .

The conversion of calibrated airspeed $v_{C,i}$ to true airspeed $v_{T,i}$ under international standard atmospheric conditions is given by Equation (18):

$$v_{T,i} = \frac{v_{C,i}}{\sqrt{(288.15 - 0.0065h_i/288.15)^{4.2579}}} \quad (18)$$

where $v_{T,i}$ and h_i represent the true airspeed and altitude, respectively, at the query point x_i .

For a sufficiently short time period Δt , the acceleration $v_T/\Delta t$ can be approximated as a constant, and the displacement Δx is linearly related to the square of time, with the underlying kinematic shown in Equation (19):

$$\Delta x = \frac{1}{2} \left(\frac{\Delta v_T}{\Delta t} \right) \times \Delta t^2 + v_{T,i} \times \Delta t \quad (19)$$

From Equations (11) and (19), the displacement with time can be approximately described by a quadratic equation, as shown in Equation (20):

$$\left[\left(\frac{T_i - D_i}{m} \right)^2 - g^2 \right] (\Delta t)^2 - \frac{2(T_i - D_i) \times \Delta v_T}{m} (\Delta t) + \Delta v_T^2 + \left(\frac{g \times \Delta x}{v_{T,i}} \right)^2 = 0 \quad (20)$$

Equation (21) demonstrates how to derive the flight time differential using the horizontal flight distance increment Δx and the differential Δv_T of the true airspeed from Equation (20):

$$\Delta t = \frac{\frac{2(T_i - D_i) \times \Delta v_T}{m} - \sqrt{\left(\frac{2(T_i - D_i) \times \Delta v_T}{m} \right)^2 - 4 \left[2 \left(\frac{T_i - D_i}{m} \right)^2 - g^2 \right] \left[\Delta v_T^2 + \left(\frac{g \times \Delta x}{v_{T,i}} \right)^2 \right]}}{2 \left[\left(\frac{T_i - D_i}{m} \right)^2 - g^2 \right]} \quad (21)$$

From Equations (11) and (20), the corresponding flight time t_i , glide path angle γ_i , altitude h_i , and fuel flow f_i are calculated iteratively, as shown in Equation (22):

$$\begin{cases} t_i = t_{i-1} + \Delta t \\ \gamma_i = \arcsin \left[\left(\frac{T_i - D_i}{m} - \frac{\Delta v_T}{\Delta t} \right) / g \right] \\ h_i = h_{i-1} + \Delta t \times v_{T,i} \times \sin \gamma_i \\ f_i = \max \left\{ C_{f1} \times \left(1 - \frac{v_{T,i}}{C_{f2}} \right) \times T, C_{f3} \times \left(1 - \frac{h_{i-1}}{C_{f4}} \right) \right\} \end{cases}, \quad (22)$$

where C_{f1} , C_{f2} , C_{f3} , and C_{f4} are the correction factors, which can all be obtained from the data in the BADA documents [44].

According to the velocity–distance profile shown in Figure 5, the state of the aircraft at each query point of the continuous descent operation can be obtained and, finally, the total fuel consumption J_{fuel} and the total flight time t_f can be calculated.

The fitness function incorporates penalty terms during evaluation, in order to ensure that the solution satisfies the constraints of the optimal control problem. The glide path angle constraint function $u(\gamma_i)$ is defined as shown in Equation (23), in order to determine whether the glide path angle is within the range:

$$u(\gamma_i) = \begin{cases} 0 & , -5 < \gamma_i < -1 \\ 1 & , \text{else} \end{cases} \quad (23)$$

In the velocity profile shown in Figure 5, the altitude $l^{(p)}$ that the aircraft must reach at $x^{(p)}$ ($p = 2, 3, 5$) follows Equation (13). In order to ascertain whether the iteratively calculated altitude meets its constraints, the altitude constraint function $y_p(h^{(p)})$ is defined as shown in Equation (24):

$$y_p(h^{(p)}) = \begin{cases} 0, & l^{(p)} - \delta < h^{(p)} < l^{(p)} + \delta \\ 1, & \text{else} \end{cases} \quad (24)$$

where δ is an allowable height tolerance. Finally, the fitness function of the GACDO model is given by Equation (25):

$$\min J_{\text{DOC}}(S) = J_{\text{fuel}} + CI \times t_f + M \times \left(\sum_{q=2,3,5} \left(y_p(h^{(p)}) \right)^2 + \sum_{i=1}^{N_1} u(\gamma_i) \right) \quad (25)$$

where M is a sufficiently large positive integer.

In accordance with the aforementioned models, a numerical solution for a continuous descent 4D trajectory-based genetic algorithm was developed in Matlab 2016b, which is referred to as the GACDO algorithm.

3. Experimental Results and Discussion

3.1. Airspace and Available Data

This study presents an example of identifying the arrival traffic flow with a point merge pattern and experiments of 4D trajectory carbon emission optimization using the airspace around Shanghai Pudong International Airport (PVG). Figure 6 provides the specific information of the airspace in detail. The PMS primarily handles arrival traffic flow from the MATNU and AND directions. Aircraft from MATNU follow standard instrument arrival route (STAR) MAT81A to enter the inner arc leg at a flight level of 2400 m. Aircraft from the AND direction follow STAR AND82A to enter the outer arc leg at a flight level of 2100 m. The maximum CAS on the arc legs must not exceed 230 kn.

ADS-B trajectory data for flights at PVG in December 2023 were acquired. The raw trajectories were pruned in accordance with the geographic boundaries of the terminal area. Departure trajectories were filtered out, and approximately 1500 arrival trajectories were retained. Radar guidance commands are frequently issued to aircraft by approach controllers for sequencing and traffic conflict resolution purposes. However, this can interfere with the aircraft's planned flight routes, causing deviations from their intended paths and resulting in more chaotic trajectories, as illustrated in Figure 6. It is important to note that this interference is a common occurrence in air traffic control. In Figure 6, solid triangles indicate compulsory reporting points for traditional navigation routes, while hollow star symbols specifically indicate non-compulsory reporting points for regional navigation routes.

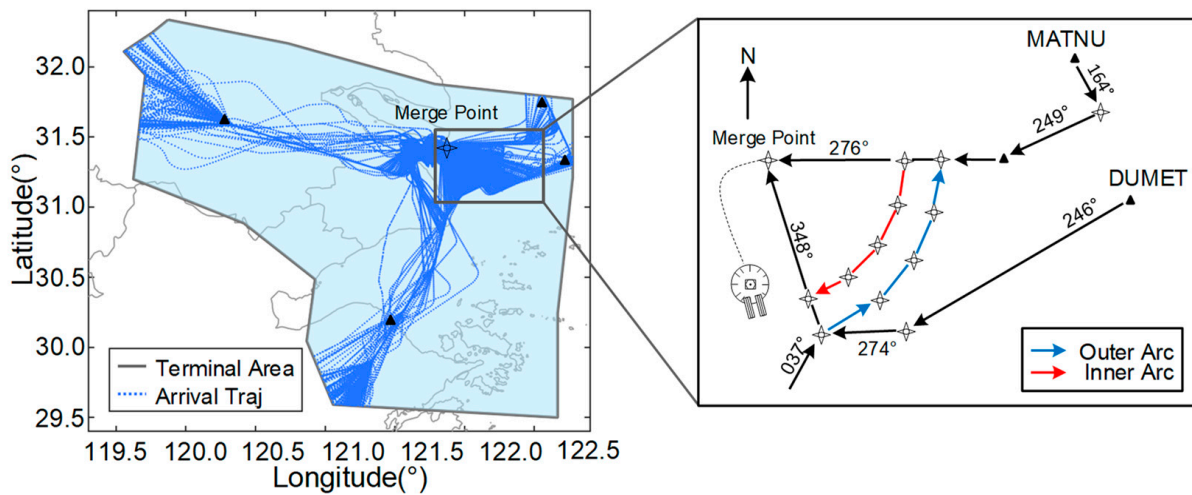


Figure 6. PVG airspace configuration and arrival trajectories.

3.2. Traffic Flow with PMS Topology and the Prevailing Arrival Route Identification

The inter-trajectory distance matrix was computed by calculating the spherical segment-path distances between arrival trajectories. The inter-trajectory similarity was then computed, taking $\sigma = 15.6$ km as the average inter-trajectory distance. A non-negative link-weighted unidirectional graph, G , was then constructed, and the Laplacian matrix of graph G was computed to have five non-zero characteristic roots. The preliminary judgment categorized the trajectories into five clusters. These clusters were then input into a spectral clustering algorithm, resulting in five arrival traffic flows, as shown in Figure 7. Among them, SASAN-01 and AND-02 follow the trombone operation pattern, denoted as F_1 and F_2 , respectively; meanwhile, MATNU-01, AND-01, and DUMET-01 follow the point merge operation pattern, denoted as F_3 , F_4 , and F_5 , respectively.

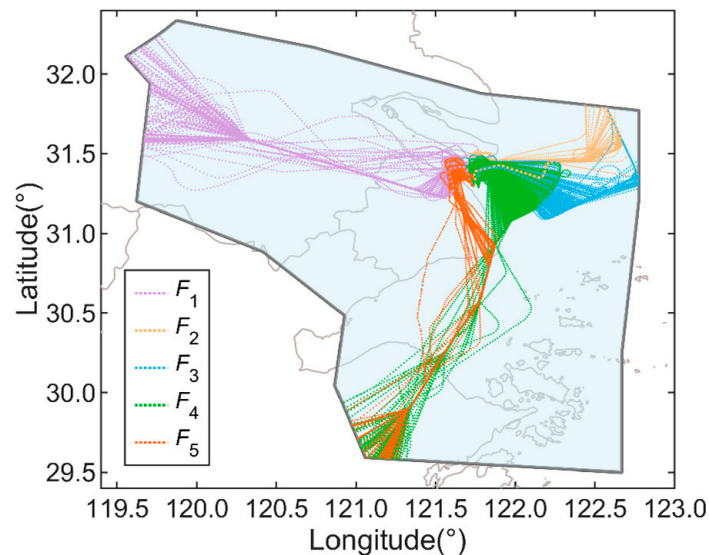


Figure 7. Five arrival traffic flows identified using spectral clustering.

Here, we take F_4 as an example. Letting $K = 11$, we calculated the distance between any trajectory in F_4 and its K nearest neighbors, then used the k -medoids method to classify the trajectories in F_4 into two categories, resulting in 377 prevailing trajectories and 14 anomalous trajectories, as shown in Figure 8. In this example, the percentage of prevailing trajectories was 96.42% and the core trajectory T_4^{ex} is shown as the blue line in Figure 8. The central trajectory is more accurate and robust, as the interference of

anomalous trajectories was eliminated. The length of the core trajectory from the terminal area boundary to the MP in this example is 202 km, of which 27 km comprises the length of the arc. These central trajectory data provide the initial conditions for the following vertical profile optimization.

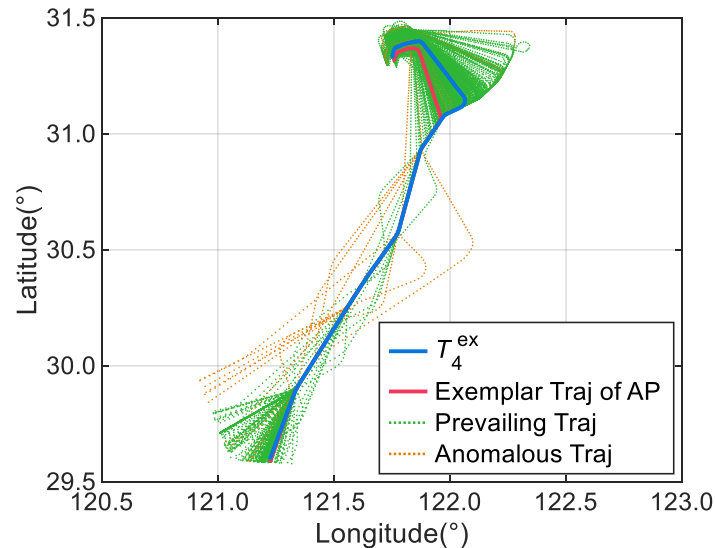


Figure 8. Comparison of core trajectories generated by k -medoids and AP clustering.

Given that determination of the representative arrival route is an essential preliminary step in the experimental process, its accuracy has a significant influence on the overall accuracy and precision of the resulting data and conclusions. In order to validate the method proposed in this study for the determination of central trajectories, a metric to measure the consistency of traffic flow trajectories—namely, the average between-like distance—is proposed. Meanwhile, the AP clustering algorithm is used for comparison. AP takes distance measures between data points as an input and, through performing the exchange of real-valued messages between data points to select an exemplary cluster center, the exemplar to which the data points belong is determined. As a result, the clusters were segmented. The trajectory clustering algorithm based on AP also identifies an exemplar trajectory, illustrated in Figure 8 as the red line.

The quality of the identified predominant traffic flow trajectories was determined according to the within-like criterion C_w . The within-like criterion was employed to illustrate the dispersion of trajectories belonging to the same traffic flow. It can be observed that arrival traffic flows with greater consistency tend to exhibit smaller within-like values, while those with less consistency exhibit larger within-like values, which is calculated according to Equation (26):

$$C_w = \frac{1}{|F_z|} \sum_{T_i \in F_z} d(T_z^{\text{ex}}, T_i). \quad (26)$$

Comparative analysis reveals that the proposed method yielded $C_w = 2.26$ km and the AP clustering method yielded $C_w = 2.39$ km. The elimination of anomalous trajectories in our method rendered the center trajectory a more suitable representative of the typical traffic flow in F_4 .

3.3. The Generation of 4D Trajectory

The arrival routes obtained in Section 3.2 were used as for the vertical profile optimization experiments which, in turn, allowed for the synthesis of a 4D trajectory for the aircraft's continuous descent operations. The experiment was conducted using an aircraft of type A320 with a CI set to 30. The initial conditions for the entry of the aircraft into the terminal airspace and the rules of operation within the terminal area are shown in Table 1.

Table 1. Initial conditions and operation rules of the A320.

h_{cr} (m)	$v_c^{(1)}$ (kn)	$x^{(0)}$ (nm)	h_{arc} (m)	$v_{C,arc}$ (kn)	h_{MP} (m)	$v_{C,MP}$ (kn)	$x^{(5)}$ (nm)	γ (°)
6900	300	-131	2100	[210, 230]	900	200	-12	[-1, -5]

The genetic algorithm had a population size of 70 and a maximum of 100 evolutionary generations. The tournament method was used to select parents for individuals that meet the constraints. The crossover operator used a single-point crossover with a probability of 0.8, and the mutation operator used a single-point mutation with a probability of 0.2.

During optimization with the GACDO algorithm, the fitness value of the optimal individual in the population stabilized after the 10th generation, indicating good convergence performance. The optimal value was 1200.89, corresponding to a fuel consumption of 528.65 kg and a flight time of 1345 s, demonstrating the effectiveness of the GACDO algorithm.

Figure 9 displays the optimized 4D trajectory results for the traffic flow cluster F_4 . The vertical profile of this trajectory is presented in Figure 9a, while Figure 9b shows the complete 4D trajectory in 3-dimensional space, integrating the horizontal trajectory and vertical profile. These data may be employed as a CO₂ emissions benchmark trajectory for the A320 aircraft type in F_4 , with benchmark emissions of 1665.25 kg.

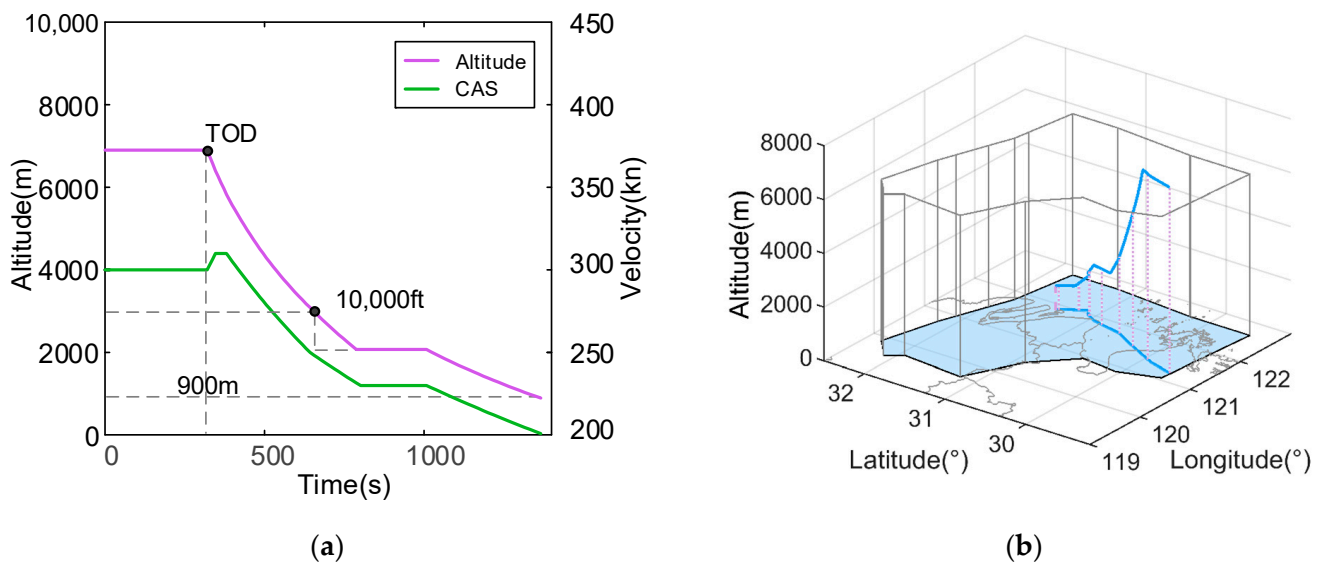


Figure 9. The optimized 4D trajectory with $CI = 30$: (a) vertical profile; and (b) optimized trajectory.

Figure 10 compares the fuel flow estimated for the real trajectory with that calculated by the GACDO algorithm. The real fuel flow was estimated using models provided by BADA. The air traffic controller instructed the aircraft to descend early, due to the inability to mentally calculate the ideal TOD, resulting in failure of the real trajectory to achieve a continuous descent operation. The extra level flight segment obviously caused a sharp increase in fuel consumption. Additionally, the shallow descent indicated a failure to reduce the thrust to close to idle, resulting in higher fuel flow. In contrast, the optimized continuous descent operation profile, with optimized TOD and selection of the ideal descent angle and velocity profile, maintained fuel consumption as low as possible, except for the level flight segments when just entering the terminal area and on the arc.

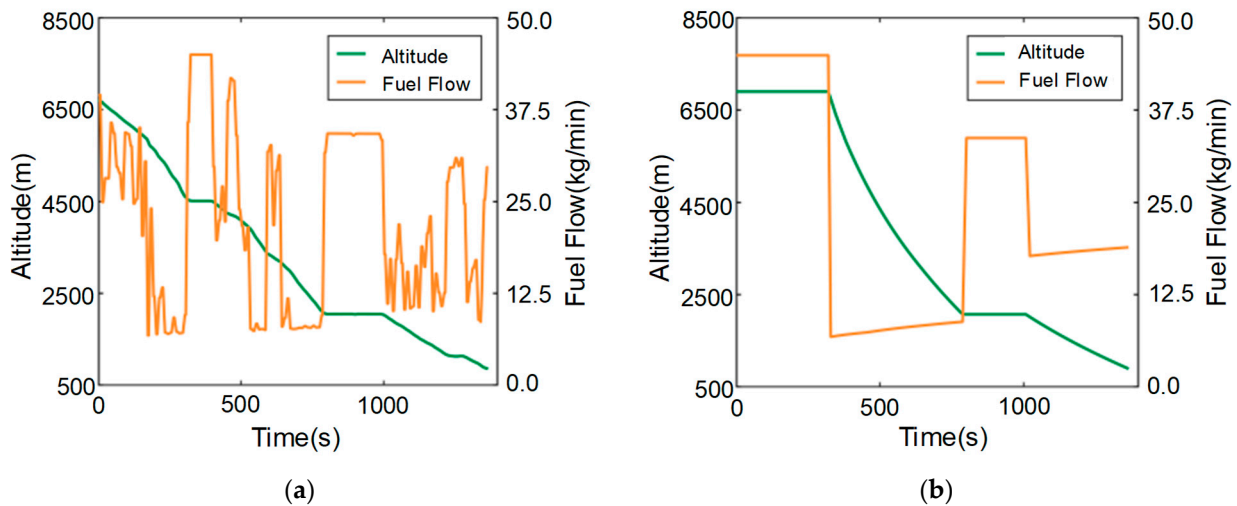


Figure 10. Fuel flow comparison: (a) real trajectory; and (b) optimized trajectory.

3.4. Comparison with Radau Pseudo-Spectral Method

The optimal control problem is typically solved using the Radau pseudo-spectral method via the MATLAB GPOPS (Version 5.0) toolbox. As illustrated in Figure 4, the PMS topology includes two descents, which must be individually optimized in GPOPS. The complete CDO profile is achieved through combining the constant velocity, level flight arc leg with the two optimized descending profiles.

Figure 11 presents a comparison of fuel consumption, CO₂ emissions, and flight time, as calculated according to the actual trajectory (T_4^{ex} in Figure 8), GPOPS, and the GACDO algorithm. The FAA’s Aviation Environmental Design Software (AEDT 3d), which is a software system that models the performance of aircraft in space and time for the estimation of fuel consumption, emissions, and noise, was utilized to calculate the results for actual trajectories. It can be observed that the endurance and CO₂ emissions of the optimized trajectories are less than those of the actual trajectory. The fuel consumptions of GPOPS and GACDO are comparable, while the flight time of GACDO is less than that of GPOPS. In contrast to GPOPS, which necessitates two distinct descent processes, GACDO depicts the arrival as a unified entity, thereby reducing the associated workload. In addition, the new method exhibits enhanced reliability through circumventing the limitations of GPOPS, which is sensitive to the initial parameter range settings.

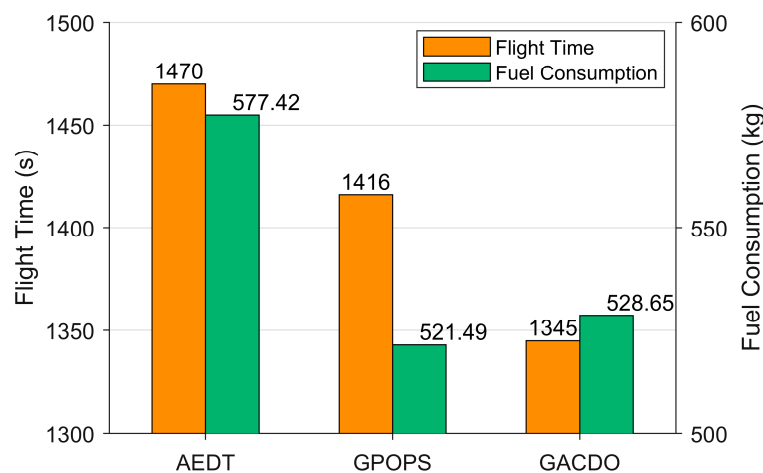


Figure 11. Comparison of results between actual trajectory and optimized trajectories.

We also compared the glide path angles derived using GPOPS and the GACDO algorithm with real trajectory, as shown in Figure 12. The results indicate that GPOPS,

which employs the Bang-Bang control strategy, tends to select the boundary value of the parameter range for the glide path angle, exhibiting a noticeable jump phenomenon. However, the glide path angle obtained with GACDO exhibits a relatively smooth trend. It is worth noting that pilots intentionally avoid steep descents for the sake of flight stability and passenger comfort. Compared to GPOPS, the GACDO algorithm can more accurately simulate the change in glide path angle in real situations, providing more reliable results. This also demonstrates the more modest optimization results obtained with GACDO.

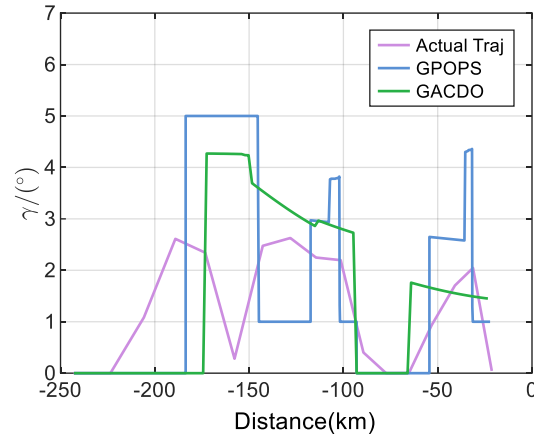


Figure 12. Comparison of glide path angles derived from GACDO, GPOPS, and the actual trajectory.

3.5. Effects of Different Cost Indices on the Optimization of 4D Trajectories

The cost index reflects the proportion of time to fuel costs in the direct operating cost. Equation (10) shows that, when the cost index is 0, the direct operating costs are concentrated on fuel consumption. In this case, the optimized vertical profile is considered the most fuel-efficient and produces the least emissions. At the maximum value of the cost index, the weights of the direct operating costs are concentrated on time costs, in which case optimization results in the smallest flight time. Different aircraft and airlines have varying ranges of cost index values, with that for the A320 model typically ranging from 0 to 100.

To compare more flight profiles using the objective function proposed in Equation (10), optimization experiments were conducted by setting *CI* values of 0, 40, and 100 for an A320 as an example. The results are shown in Figure 13.

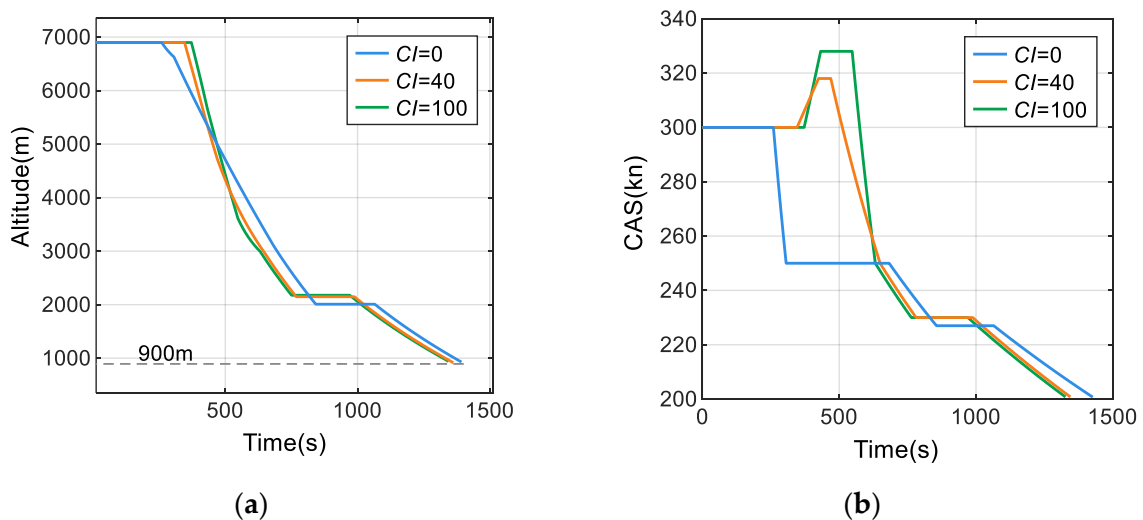


Figure 13. Trajectory optimization results for different *CI* values: (a) altitude profile; and (b) CAS profile.

Figure 13a illustrates that, when CI is equal to 0, the optimization objective becomes Equation (8), which minimizes fuel consumption and CO_2 emissions during the descent operation. Conversely, when $CI = 100$, the optimization objective becomes Equation (9), which minimizes the time taken for the trajectory. When CI is equal to 40, the direct operating cost of the trajectory is minimized by considering both the time and fuel costs, as shown in Equation (10). The larger the CI , the later the TOD, the steeper the altitude profile, and the shorter the flight time. As the CI value increases, the altitude profile gradually approaches the profile of minimum time. The smaller the CI value, the earlier the TOD, and the altitude profile becomes relatively shallow, resulting in reduced fuel consumption and emissions.

Figure 13b illustrates that, when $CI = 0$, the aircraft tends to fly at a lower CAS after passing the TOD point to minimize fuel consumption. However, the minimum CAS limitation of 250 kn above 10,000 ft restricts the deceleration target to 250 kn at this stage. The aircraft cannot further decelerate until below 10,000 ft. It was found that the velocity profile trend remained consistent across different CI values, with the exception of a slightly unusual profile at $CI = 0$. As the value of CI increases, the velocity profile becomes steeper and v_1 increases. The aircraft maintains its maximum velocity during descent to minimize the flight time.

The above analysis shows that, under the condition of a given arrival route, the GACDO algorithm can dynamically adjust the top of descent, velocity profile, and glide path angle according to the different optimization objectives, thus accomplishing 4D trajectory optimization for continuous descent operations.

3.6. The Environmental Efficiency Gaps of Traffic Flow F_4

It is widely acknowledged that an inappropriate flight altitude is a significant contributor to increased fuel consumption and greenhouse gas emissions. Figure 14 illustrates a comparison between the altitude profiles of the actual trajectory and the optimized 4D trajectory in traffic flow F_4 , which reveals a noticeable deviation between the trajectory's actual altitude profile and the ideal altitude profile, which is the primary cause of the additional emissions. Air traffic controllers often instruct aircraft to descend earlier, due to their inability to accurately determine the position of the TOD. This can result in a low-altitude level flight segment and a shadow descent slope. The trajectories of aircraft of type A320 in Figure 14 have longer level flights at several flight levels, such as 2400 m, 4200 m, and 6100 m. Additionally, the on-board FMS attempts to intercept the ideal descent profile during the descent, resulting in a smaller descent gradient in the actual trajectory, as compared to the optimized continuous descent gradient.

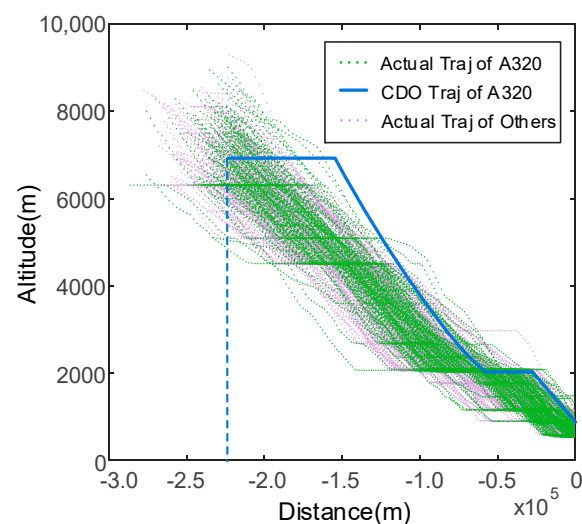


Figure 14. Comparison of actual and optimized altitude profiles in arrival traffic flow F_4 .

Table 2 shows the environmental efficiency gaps of the arrival traffic flow cluster F_4 . Flight time, fuel consumption, and CO₂ emissions were calculated according to the aircraft types and their trajectories using AEDT. The vertical profiles of the predominant arrival routes were optimized according to the performance parameters associated with the aircraft type, which can be used as an emissions benchmark for traffic flow cluster F_4 .

Table 2. The environmental efficiency gaps of F_4 .

Aircraft Type	CI	Actual Trajectories			Optimized Trajectories		
		Num	Average Fuel /CO ₂ (kg)	Average Flight Time (s)	l_{TOD} (km)	Fuel/CO ₂ (kg)	Flight Time (s)
A320	30	214	551.7/1737.8	1479	−174.4	528.7/1665.4	1345
A333	45	31	1105.4/3481.9	1449	−183.6	958.1/3018.0	1367
A343	45	6	1344.6/4235.6	1495	−189.2	1160.2/3654.6	1376
B738	20	112	556.9/1754.3	1507	−170.7	542.6/1709.2	1382
B773	120	28	1418.8/4469.4	1524	−178.1	1346.73/4242.1	1363

Analysis of the data presented in Figure 14 and Table 2 indicates that, when each aircraft type uses their usual cost indices, the time required for aircraft following the optimal 4D trajectory is reduced by an average of 8%. Additionally, fuel consumption and CO₂ emissions are reduced by an average of 10%, resulting in a significant reduction in emissions and efficiency benefits.

The analysis demonstrated that the 4D trajectory optimization method proposed in this study provides a benchmark for CO₂ emissions, which can be used for the scientific evaluation of environmental efficiency. This can help air traffic management operators to monitor environmental performance and adopt targeted improvement techniques, and contributes to the eventual achievement of the goal of carbon peaking in the air transport industry.

4. Conclusions

This study proposed a 4D trajectory optimization method for the CO₂ emission benchmarking of arrival traffic flows with PMS topology. The proposed methodology achieves two improvements over traditional methods. First, we proposed a data-driven and optimal control model combined approach to benchmark CO₂ emissions from the perspective of the arrival traffic flow, rather than from the perspective of the entire terminal airspace. This may contribute to targeted improvements in airspace design and ATM. Second, the whole arrival descent profile of the PMS topology is divided into two correlated descent processes using a level flight arc leg, and a holistic and unified modeling and solution method for multiple descent processes is proposed. This method overcomes the inefficiency of the pseudo-spectral method in terms of modeling the two descent processes separately.

The proposed 4D trajectory optimization method for CO₂ benchmarking was applied to a realistic terminal airspace setting, and its applicability was verified through two successive experiments. The results of the first experiment indicated that 3.58% of the trajectories within arrival traffic flow F_4 exhibited inconsistencies. After removing these anomalous trajectories, the within-like criterion of the traffic flow F_4 was reduced to 2.26 km, making it more suitable for generating representative arrival routes. In the second experiment, vertical profile optimization was conducted, considering parameters such as different cost indices and different aircraft models. The experimental results demonstrated that the proposed method is adaptable to variation in the aforementioned parameters, and can successfully generate respective vertical profiles. For the arrival traffic flow F_4 , a reference trajectory for carbon emissions was generated for the A320 aircraft, with a benchmark emission of 1665.25 kg when the cost index was set to 30. The results also indicate an environmental efficiency gap of approximately 10% between the actual CO₂ emissions of the traffic flow and the obtained benchmark.

The 4D trajectory optimization method proposed in this study was constructed on the premise of international standard atmospheric conditions and without consideration of wind. Future work will incorporate a wind field model of the terminal airspace in order to more realistically simulate the real flight environment, thereby achieving more accurate trajectory optimization. In addition, the potential for optimizing the PMS structure itself to reduce greenhouse gas emissions can also be explored.

Author Contributions: Conceptualization, C.W. and S.S.; methodology, C.W.; software, C.W. and W.L.; validation, S.L., W.L. and C.X.; formal analysis, W.L.; investigation, C.W. and C.X.; resources, C.W.; data curation, C.W.; writing—original draft preparation, C.W. and C.X.; writing—review and editing, C.W.; visualization, C.X. and W.L.; supervision, C.W.; project administration, C.W.; funding acquisition, C.W. All authors have read and agreed to the published version of the manuscript.

Funding: This research was funded by the key project of applied basic research multi-investment fund of Tianjin municipal (No. 21JCZDJC00780).

Data Availability Statement: The raw data supporting the conclusions of this article will be made available by the authors on request.

Acknowledgments: We would like to thank the Tianjin Hangda Data Co., Ltd.—aviationX for providing the ADS-B data used in the model tests described in this paper.

Conflicts of Interest: The authors declare no conflicts of interest.

References

1. Klöwer, M.; Allen, M.; Lee, D.; Proud, S.; Gallagher, L.; Skowron, A. Quantifying aviation's contribution to global warming. *Environ. Res. Lett.* **2021**, *16*, 104027. [[CrossRef](#)]
2. ICAO. *2016–2030 Global Air Navigation Plan (Doc 9750-AN/963)*; International Civil Aviation Organization: Montréal, QC, Canada, 2016.
3. Reynolds, T.G. Air traffic management performance assessment using flight inefficiency metrics. *Transp. Policy* **2014**, *34*, 63–74. [[CrossRef](#)]
4. Todoric, M.; Mastelic, T. Comparison of Similarity Measures for Trajectory Clustering—Aviation Use Case. *J. Commun. Softw. Syst.* **2023**, *19*, 178–187. [[CrossRef](#)]
5. Chu, X.; Tan, X.; Zeng, W. A Clustering Ensemble Method of Aircraft Trajectory Based on the Similarity Matrix. *Aerospace* **2022**, *9*, 269. [[CrossRef](#)]
6. Besse, P.; Guillouet, B.; Loubes, J.-M.; François, R. Review and perspective for distance based trajectory clustering. *arXiv* **2015**, arXiv:1508.04904. [[CrossRef](#)]
7. Poppe, M.; Buxbaum, J. Clustering climb profiles for vertical trajectory analysis. In Proceedings of the 10th SESAR Innovation Days, Virtual, 7–10 December 2020; pp. 7–10.
8. Xiao, Y.; Ma, Y.; Ding, H.; Xu, Q. Flight trajectory clustering based on a novel distance from a point to a segment set. In Proceedings of the Fourth International Workshop on Pattern Recognition, Nanjing, China, 28–30 June 2019; pp. 68–73.
9. Olive, X.; Morio, J. Trajectory clustering of air traffic flows around airports. *Aerosp. Sci. Technol.* **2019**, *84*, 776–781. [[CrossRef](#)]
10. Gui, X.; Zhang, J.; Peng, Z. Trajectory clustering for arrival aircraft via new trajectory representation. *J. Syst. Eng. Electron.* **2021**, *32*, 473–486. [[CrossRef](#)]
11. Zeng, W.; Xu, Z.; Cai, Z.; Chu, X.; Lu, X. Aircraft trajectory clustering in terminal airspace based on deep autoencoder and gaussian mixture model. *Aerospace* **2021**, *8*, 266. [[CrossRef](#)]
12. Wang, Z.-S.; Zhang, Z.-Y.; Cui, Z. Research on Resampling and Clustering Method of Aircraft Flight Trajectory. *J. Signal Process. Syst.* **2022**, *95*, 319–331. [[CrossRef](#)]
13. Murça, M.C.R.; Guterres, M.X.; de Oliveira, M.; Szczenek, J.B.T.; Souza, W.S.S.A. Characterizing the Brazilian airspace structure and air traffic performance via trajectory data analytics. *J. Air Transp. Manag.* **2020**, *85*, 101798. [[CrossRef](#)]
14. Zhang, Z.; Zhang, A.; Sun, C.; Guan, J.; Huang, X. The Reliability Analysis of Air Traffic Network Based on Trajectory Clustering of Terminal Area. *IEEE Access* **2020**, *8*, 75035–75042. [[CrossRef](#)]
15. Ben-Asher, J.Z. *Optimal Control Theory with Aerospace Applications*; American Institute of Aeronautics and Astronautics: Reston, VA, USA, 2010. [[CrossRef](#)]
16. Betts, J.T. Survey of numerical methods for trajectory optimization. *J. Guid. Control Dyn.* **1998**, *21*, 193–207. [[CrossRef](#)]
17. Bellman, R. Dynamic programming. *Science* **1966**, *153*, 34–37. [[CrossRef](#)] [[PubMed](#)]
18. Miyamoto, Y.; Wickramasinghe, N.K.; Harada, A.; Miyazawa, Y.; Funabiki, K. Analysis of fuel-efficient airliner flight via dynamic programming trajectory optimization. *Trans. Jpn. Soc. Aeronaut. Space Sci. Aerosp. Technol. Jpn.* **2013**, *11*, 93–98. [[CrossRef](#)]
19. Bousson, K. Single gridpoint dynamic programming for trajectory optimization. In Proceedings of the AIAA Atmospheric Flight Mechanics Conference and Exhibit, San Francisco, CA, USA, 15–18 August 2005; p. 5902.

20. Harada, A.; Matsuda, H.; Miyazawa, Y. Dynamic programming trajectory optimization by piecewise linear approximation. In Proceedings of the AIAA Guidance, Navigation, and Control Conference, Kissimmee, FL, USA, 5–9 January 2015; p. 1075.
21. Miyazawa, Y.; Wickramasinghe, N.K.; Harada, A.; Miyamoto, Y. Dynamic programming application to airliner four dimensional optimal flight trajectory. In Proceedings of the AIAA Guidance, Navigation, and Control (GNC) Conference, Boston, MA, USA, 19–22 August 2013; p. 4969.
22. Ahmed, K.; Bousson, K.; Coelho, M.d.F. A modified dynamic programming approach for 4D minimum fuel and emissions trajectory optimization. *Aerospace* **2021**, *8*, 135. [[CrossRef](#)]
23. Burrows, J.W. Fuel-optimal aircraft trajectories with fixed arrival times. *J. Guid. Control Dyn.* **1983**, *6*, 14–19. [[CrossRef](#)]
24. Chakravarty, A. Four-dimensional fuel-optimal guidance in the presence of winds. *J. Guid. Control Dyn.* **1985**, *8*, 16–22. [[CrossRef](#)]
25. Tang, G.; Jiang, F.; Li, J. Fuel-optimal low-thrust trajectory optimization using indirect method and successive convex programming. *IEEE Trans. Aerosp. Electron. Syst.* **2018**, *54*, 2053–2066. [[CrossRef](#)]
26. Franco, A.; Rivas, D. Optimization of multiphase aircraft trajectories using hybrid optimal control. *J. Guid. Control Dyn.* **2015**, *38*, 452–467. [[CrossRef](#)]
27. Betts, J.T.; Cramer, E.J. Application of direct transcription to commercial aircraft trajectory optimization. *J. Guid. Control Dyn.* **1995**, *18*, 151–159. [[CrossRef](#)]
28. Tian, Y.; He, X.; Xu, Y.; Wan, L.; Ye, B. 4D trajectory optimization of commercial flight for green civil aviation. *IEEE Access* **2020**, *8*, 62815–62829. [[CrossRef](#)]
29. Soler, M.; Olivares, A.; Staffetti, E.; Zapata, D. Framework for aircraft trajectory planning toward an efficient air traffic management. *J. Aircr.* **2012**, *49*, 341–348. [[CrossRef](#)]
30. Soler, M.; Olivares, A.; Staffetti, E. Multiphase optimal control framework for commercial aircraft four-dimensional flight-planning problems. *J. Aircr.* **2015**, *52*, 274–286. [[CrossRef](#)]
31. Bonami, P.; Olivares, A.; Soler, M.; Staffetti, E. Multiphase mixed-integer optimal control approach to aircraft trajectory optimization. *J. Guid. Control Dyn.* **2013**, *36*, 1267–1277. [[CrossRef](#)]
32. Li, W.; Yang, L.; Chen, Y.; Zhang, H.; Zhao, Z. Multi-Objective Optimization of CDO Trajectory in a Flexible Airspace Structure. In Proceedings of the 2020 Integrated Communications Navigation and Surveillance Conference (ICNS), Herndon, VA, USA, 8–10 September 2020; pp. 3C3–1–3C3-15.
33. Yang, L.; Li, W.; Wang, S.; Zhao, Z. Multi-attributes decision-making for CDO trajectory planning in a novel terminal airspace. *Sustainability* **2021**, *13*, 1354. [[CrossRef](#)]
34. Park, S.G.; Clarke, J.-P. Optimal control based vertical trajectory determination for continuous descent arrival procedures. *J. Aircr.* **2015**, *52*, 1469–1480. [[CrossRef](#)]
35. Park, S.G.; Dutta, P.; Menon, P. Optimal Trajectory Option Sets for In-Flight Climb-Descend Trajectory Negotiations. In Proceedings of the 17th AIAA Aviation Technology, Integration, and Operations Conference, Denver, Colorado, 5–9 June 2017; p. 3432.
36. Ma, L.; Tian, Y.; Zhang, Y.; Chu, P. Trajectory Optimization of Aircraft for A Continuous Descent Continuous Procedure. In Proceedings of the 2020 Chinese Automation Congress (CAC), Shanghai, China, 6–8 November 2020; pp. 2063–2067.
37. Zhiqiang, Z.; Yaoguang, D.; Fenxun, G.; Qidong, Y. Research on CDO Trajectory Optimization Based on Cost Index using Gaussian Pseudospectral Method. In Proceedings of the International Workshop on ATM/CNS 2022 International Workshop on ATM/CNS, Tokyo, Japan, 25–27 October 2022; pp. 164–169.
38. Wang, C.; Chen, H.; Qin, H.; Liu, B. A 4D Trajectory Prediction Method of Continuous Descent Operation in Congested Terminal Control Area. *J. Southwest Jiaotong Univ.* **2024**. Available online: <https://link.cnki.net/urlid/51.1277.U.20231204.1042.008> (accessed on 4 December 2023).
39. Yang, C.; Yu, Y.; Li, Q.; Ren, Z. Trajectory optimization for arrival aircraft using a hybrid IPSO-SQP algorithm. In Proceedings of the 2016 IEEE Chinese Guidance, Navigation and Control Conference (CGNCC), Nanjing, China, 12–14 August 2016; pp. 2159–2163.
40. Morante, D.; Sanjurjo Rivo, M.; Soler, M. A Survey on Low-Thrust Trajectory Optimization Approaches. *Aerospace* **2021**, *8*, 88. [[CrossRef](#)]
41. Ren, G.; He, J. Research on Aircraft Green Trajectory Optimization for Terminal Area. *J. Beijing Univ. Aeronaut. Astronaut.* **2024**, *48*, 12. [[CrossRef](#)]
42. Putra, R.H.D.; Sujiani, H.; Safriadi, N. Penerapan Metode Haversine Formula Pada Sistem Informasi Geografis Pengukuran Luas Tanah. *J. Sist. Dan Teknol. Inf. (JUSTIN)*. **2015**, *1*, 1–6.
43. Budd, T.; Suau-Sanchez, P. Assessing the fuel burn and CO2 impacts of the introduction of next generation aircraft: A study of a major European low-cost carrier. *Res. Transp. Bus. Manag.* **2016**, *21*, 68–75. [[CrossRef](#)]
44. Nuic, A.; Poles, D.; Mouillet, V. BADA: An advanced aircraft performance model for present and future ATM systems. *Int. J. Adapt. Control Signal Process.* **2010**, *24*, 850–866. [[CrossRef](#)]

Disclaimer/Publisher’s Note: The statements, opinions and data contained in all publications are solely those of the individual author(s) and contributor(s) and not of MDPI and/or the editor(s). MDPI and/or the editor(s) disclaim responsibility for any injury to people or property resulting from any ideas, methods, instructions or products referred to in the content.